Available online at www.sciencedirect.com
SCIENCE DIRECT
Polymer 46 (2005) 10191–10201
polymer
www.elsevier.com/locate/polymer

Structure–property behavior of segmented polyurethaneurea copolymers based on an ethylene–butylene soft segment

Derek B. Klinedinst[a], Emel Yilgör[b], Iskender Yilgör[b], Frederick L. Beyer[c], Garth L. Wilkes[d,*]

[a]Department of Materials Science and Engineering, Virginia Polytechnic Institute and State University, Blacksburg, VA 24061, USA
[b]Department of Chemistry, Koc University, Istanbul 34450, Turkey
[c]US Army Research Laboratory, Materials Division, Aberdeen Proving Grounds, Aberdeen, MD 21005, USA
[d]Polymer Materials and Interfaces Laboratory, Department of Chemical Engineering, Virginia Polytechnic Institute and State University, Blacksburg, VA 24061, USA

Received 12 May 2005; accepted 19 July 2005
Available online 1 September 2005

Abstract

Novel segmented polyurethaneurea copolymers were synthesized using a poly(ethylene–butylene) glycol based soft segment and either hydrogenated diphenyl methane diisocyanate (HMDI) or hexamethylene diisocyanate (HDI) in addition to either ethylene diamine (EDA) or 2-methyl-1,5-diaminopentane (DY) as the chain extender. Dynamic mechanical analysis (DMA), small angle X-ray scattering (SAXS) and in some cases atomic force microscopy (AFM) established the presence of a microphase-separated structure in which hard microdomains are dispersed throughout a soft segment matrix. Wide angle X-ray scattering (WAXS) and differential scanning calorimetry (DSC) imply that the materials are amorphous. Samples that are made with HMDI/DY and have hard segment contents in the range of 16–23 wt% surprisingly exhibit near-linear mechanical deformation behavior in excess of 600% elongation. They also show very high levels of recoverability even though their hysteresis is also considerable. The materials have all proven to be melt processable in addition to solution processable.

Keywords: Polyurethaneurea; Morphology; Properties

1. Introduction

Segmented block copolymers are widely used in several industries including automotive coatings, molded components, sporting goods manufacturing, and in the insulation business [1,2]. The breadth in the applications for these materials can be attributed in part to their wide range of mechanical and thermal properties. That these properties can be controlled and even tailored to a specific end use makes segmented copolymers a very attractive class of materials.

As a group, segmented thermoplastic polyurethanes, polyureas and polyurethaneureas (TPUs) are a subclass of linear segmented copolymers possessing a backbone comprised of alternating soft segments (SS) and hard segments (HS). These segments typically have rather low molecular weights compared to triblock copolymers, such as the styrene–butadiene–styrene (SBS) systems, which generally possess block molecular weights of 10,000–100,000 g/mol and are prepared by anionic polymerization [3,4]. The soft segments in TPUs are often, but not exclusively, polyethers or polyesters and are chosen based on desired functionality, reactivity and molecular weight. The hard segment, also low in molecular weight, is typically formed from the reaction of a diol or diamine chain extender with excess diisocyanate. The isocyanates are either aromatic or aliphatic and the choice is based on a number of factors including cost and reactivity. The specific chemistry and symmetry of the isocyanate has been shown to affect ultimate properties of the materials, and careful consideration must be given to this choice [5,6]. Diamines are common chain extender molecules used in the synthesis of urea linkages, although other moieties such as water can also be used as is common in the production of 'polyurethane' flexible foams [7].

Linear polyurethaneureas are synthesized using a step growth reaction technique first developed by Otto Bayer in

* Corresponding author. Tel.: +1 540 231 5498; fax: +1 540 231 8511.
E-mail address: gwilkes@vt.edu (G.L. Wilkes).

0032-3861/$ - see front matter © 2005 Elsevier Ltd. All rights reserved.
doi:10.1016/j.polymer.2005.07.065

the late 1930s [7]. In the more commonly used prepolymer method, linear hydroxyl terminated oligomeric polyether or polyesters are reacted with an excess of a selected diisocyanate to cap the oligomer thereby forming a urethane linkage and leaving an isocyanate functional group at each terminus, forming what is termed a 'prepolymer'. This prepolymer mixture (containing additional diisocyanate) is then reacted with a diamine chain extender to form the hard segments and increase the molecular weight of the macromolecule. In general, an increase in HS content leads to increased modulus (stiffness) and enhanced tensile strength [8,9].

The wide range of properties of segmented copolymers is credited to microphase-separation, the process whereby hard segments segregate, forming hard microdomains in a matrix of soft segments. These microdomains are generally well dispersed throughout the soft segment matrix and act as physical cross-links adding modulus, stiffness and strength. In block copolymer materials with non-specific interactions, an examination of the Flory–Huggins χ parameter helps define under what conditions microphase-separation will occur [10]. Such an approach, however, cannot easily be utilized in the present case due to specific molecular interactions promoted by hydrogen bonding between the urethane and urea groups in the HS of these materials.

The soft segment phase of these materials usually has a glass transition temperature (T_g) well below room temperature and it is this phase in thermoplastic polyurethanes, polyureas and polyurethaneureas that lowers the elastic modulus and enhances elongational properties. If microphase-separation occurs and the hard phase is also well-percolated throughout the material, the percolation will have the effect of further increasing modulus for a given composition, but it will also promote the potential for yielding and enhanced mechanical hysteresis. In urea HS containing systems, the HS microdomains can provide further strength to the material through the development of a bidentate hydrogen bonded network, through intra- or intermolecular interactions. Calculations have shown the bond energy of bidentate hydrogen bonds to be 21.8 kJ/mol [11]. In contrast, polyurethane systems can only display a monodentate hydrogen bonded network between urethane groups on the same or adjacent chains and posses a lower bond energy of 18.4 kJ/mol. The hard segments of polyurethanes or polyureas can also display crystallization if the appropriate process history is utilized and HS symmetry exists. In contrast to the conventional polyether or polyester polyols, the soft segment used in the present study is an ethylene–butylene based polyol, Kraton™ Liquid L-2203. This ethylene–butylene oligomer was synthesized by the hydrogenation of an α,ω-hydroxy terminated polybutadiene, which was prepared by anionic polymerization. The resulting amorphous SS has no significant polarity compared to polyester or polyether based systems. It also differs in that the SS molecular weight is 3340 g/mol as opposed to typical values of 1000–2000 g/mol used in the majority of linear segmented polyurethanes and polyurethaneureas. Both of these features imply that microphase separation will be strongly favored for typical hard segments based on polyurethane or polyurea chemistry. In preparing the linear segmented copolymers studied here, two different diisocyanates were employed: hydrogenated diphenyl methane diisocyanate (HMDI) and hexamethylene diisocyanate (HDI). The chain extenders chosen were ethylene diamine (EDA) and 2-methyl-1,5-diaminopentane which is sold under the name Dytek® (DY). The chemical structures for both the diisocyanates and chain extenders are given in Scheme 1. These constituents allowed the examination of the role of symmetry in the behavior of linear segmented polyurethaneureas, as EDA is a symmetric molecule but DY is asymmetric.

This study has two foci. First, the properties of segmented polyurethaneurea films comprised of a non-polar ethylene–butylene (EB) soft segment and an HMDI–DY hard segment are examined. Particular attention is given to the way solid-state properties are affected by HS content in the range (16–23 wt%). Second, an investigation is made into the effect the choice of chain extender has on the properties of ethylene–butylene soft segment based polyurethaneureas. Here, HDI is employed as the diisocyanate and the chain extender used is either EDA or DY.

2. Experimental

2.1. Materials

Bis(4-isocyanatocyclohexyl)methane (HMDI) (Bayer) and 1,6-hexamethylene diisocyanate (HDI) (Aldrich) with purities of greater than 99.5% were used. Hydroxy terminated Kraton™ Liquid-L-2203 was kindly supplied by Kraton Inc. The average functionality and the number average molecular weight ($\langle M_n \rangle$) of Kraton™ L-2203, as determined by ^{1}H NMR, were 1.92 and 3340 g/mol, respectively. It also had a very narrow molecular weight distribution of 1.03, as determined by SEC. Reagent grade ethylene diamine (EDA) was purchased from Aldrich. 2-Methyl-1,5-diaminopentane (DY) was kindly provided by Du Pont. HPLC grade toluene, isopropyl alcohol (IPA), and tetrahydrofuran (THF) (Aldrich) were all used as received. The catalyst, dibutyltin dilaurate (T-12) is a product of Witco.

2.2. Polymer synthesis

Polymerizations were conducted in three-neck, round bottom, Pyrex reaction flasks equipped with an overhead stirrer, addition funnel and nitrogen inlet. All copolymers were prepared by using the two-step, prepolymer method. To prepare the prepolymer, calculated amounts of diisocyanate and Kraton™ L-2203 were introduced into the reactor, stirred and heated. When the mixture reached 80 °C,

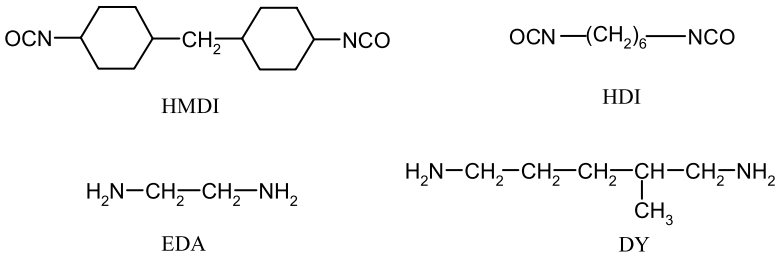

Scheme 1.

200 ppm of dibutyltin dilaurate (T-12) in toluene was added as catalyst. Prepolymer formation was monitored by FTIR spectroscopy, following the disappearance of the broad hydroxyl stretching peak around 3450 cm^{-1} and formation of the N–H peak and C=O peaks near 3300 and 1720 cm^{-1}, respectively. After the completion of prepolymer formation, the system was cooled to ambient conditions and the prepolymer was dissolved in toluene or THF. Then it was further cooled to 0 °C in an ice-water bath and diluted with isopropyl alcohol. For chain extension, a stoichiometric amount of diamine chain extender (DY or EDA) was weighed into an Erlenmeyer flask, dissolved in IPA, introduced into the addition funnel and added dropwise into the prepolymer solution at 0 °C, under strong agitation. Completion of reactions was determined by monitoring the disappearance of the isocyanate absorption peak around 2270 cm^{-1} with a FTIR spectrophotometer. Reaction mixtures were homogeneous and clear throughout the polymerizations.

Table 1 provides the compositional characteristics of the poly(ethylene–butylene)glycol based polyurethaneureas prepared in this study. SS chain length is constant at 3340 g/mol. HS chain length, as shown on the last column of Table 1 varies between 280 and 1020 g/mol, depending on the hard segment content. The convention for sample designation used is as follows: Diisocyanate/chain extender/HS wt%. Therefore, HMDI/DY/16 refers to a polyurethaneurea with an ethylene/butylene SS, HMDI and DY chain extender with a HS content of 16.2 wt%. HDI/DY/9 and HDI/EDA/8 have identical molar compositions. The small difference in HS content is due to the difference in the molecular weight of the diamine.

Table 1
Compositions and average hard segment lengths of poly(ethylene–butylene)glycol (M_n = 3340 g/mol) based polyurethaneurea copolymers

Sample code	Diisocyanate	Chain extender	HS content (wt%)	HS $\langle M_n \rangle$ (g/mol)
HMDI/DY/16	HMDI	DY	16.2	645
HMDI/DY/19	HMDI	DY	19.4	800
HMDI/DY/23	HMDI	DY	23.4	1020
HDI/DY/9	HDI	DY	8.7	320
HDI/EDA/8	HDI	EDA	7.8	280

Higher values of HS content were prevented due to solubility issues caused by the lengthening of the urea HS. Solution based films were cast from a toluene/IPA mixture into Teflon molds, covered with glassware to slow down the solvent evaporation, and placed into a 60 °C oven overnight. The molds were then removed from the drying oven and placed into a vacuum oven at room temperature for at least 2 days to complete the solvent removal. The samples were kept under vacuum at room temperature when not in use. Interestingly, all films were also compression moldable at 200 °C, at ca. 300 psi resulting in clear, monolithic, uniform films.

2.3. Atomic force microscopy (AFM)

AFM was performed using a Digital Instruments (now Veeco) Dimension 3000 atomic force microscope with a NanoScope IIIa controller. The microscope was operated at ambient temperature in the tapping mode using Nanodevices TAP150 silicon cantilever probe tips. The tips possessed a 5 N/m spring constant and a resonant frequency of ca. 100 kHz. The free air amplitude was normally set at 2.8 V. Some samples, however, necessitated the use of a much higher free air amplitude of ca. 8.0 V. The tapping force was varied by controlling the set point for each scan and was varied depending on sample conditions. Typically, a value was chosen so that the set point ratio fell in the range 0.4–0.7, constituting hard to medium tapping strengths. Scans were done at a frequency of 1 Hz.

2.4. Dynamic mechanical analysis (DMA)

DMA was performed on a Seiko DMS 210 tensile module with an attached auto-cooler for precise temperature control. Rectangular samples measuring 10 mm in length and 4.5–6.5 mm in width were cut from the cast films. Under a dry nitrogen atmosphere, the films were deformed using a frequency of 1 Hz. The temperature was increased from −150 to 200 °C at a rate of 2 °C/min. Soft segment glass transition temperatures reported by the DMA methodology were denoted as the location of the peak in the tan δ versus temperature plots.

2.5. Tensile testing

The stress–strain behavior of the films was measured using an Instron Model 4400 Universal Testing System controlled by Series IX software. A bench-top die was used to cut 2.91×10 mm dogbone samples from the larger cast films. These dogbones were then tested to failure at a crosshead speed of 25 mm/min and their load versus displacement values recorded. Three samples were measured and their results were averaged to determine modulus, yield strength, and strain-at-break for each of the five materials. In addition to testing the materials to failure, hysteresis measurements were also made. For this test, the dogbone shaped samples were stretched to 600% strain at a crosshead speed of 25 mm/min and then immediately returned to its initial position of 0% strain at the same rate. This loading–unloading cycle was repeated twice more to produce a three-cycle hysteresis test. Lastly, an Instron was also used to perform stress relaxation experiments. In this case, the sample was rapidly stretched to a strain of either 25 or 600% and held while the decay in load as a function of time was recorded.

2.6. Wide angle X-ray scattering (WAXS)

Photographic flat WAXS studies were performed using a Philips PW 1720 X-ray diffractometer emitting Cu K_α radiation with a wavelength of $\lambda = 1.54$ Å. The operating voltage was set to 40 kV and the tube current set to 20 mA. The sample to film distance was set at 47.3 mm for all samples. Direct exposures were made using Kodak Biomax MS film in an evacuated sample chamber. X-ray exposures lasted 4 h. Sample thickness ranged from 12–14 mils for the three HMDI/DY samples and 19.5–20 mils for the HDI/ED and HDI/DY samples.

2.7. Small angle X-ray scattering (SAXS)

Pin-hole collimated SAXS profiles were collected at ambient temperature using a Rigaku Ultrax18 rotating anode X-ray generator operated at 40 kV and 60 mA. A pyrolytic graphite monochromator was used to filter out all radiation except the Cu K_α doublet, with an average wavelength of $\lambda = 1.5418$ Å. The camera used 200, 100 and 300 μm pinholes for X-ray collimation. Two-dimensional data sets were collected using a molecular metrology 2D multi-wire area detector, located approximately 65 cm from the sample. After azimuthal averaging, the raw data were corrected for detector noise, sample absorption, and background noise. The data were then placed on an absolute scale using a 1.07 mm thick type 2 glassy carbon sample, previously calibrated at the Advanced Photon Source at the Argonne National Laboratory, as a secondary standard. All the SAXS profiles presented have been masked in the low scattering vector region where the beam stop influenced the profiles. The absolute intensity data are presented as a function of the magnitude of the scattering vector, s, where $s = 2\sin(\theta)/\lambda$, and 2θ is the scattering angle.

2.8. Differential scanning calorimetry (DSC)

DSC was used to determine potential melting behavior of the segmented polyurethaneureas and was also used as a second method for determining SS glass transition temperatures. DSC experiments were conducted on a Seiko DSC 220C with an attached auto-cooler for precise temperature control. Samples weighing 10–15 mg were heated in a nitrogen atmosphere from −150 to 200 °C at 10 °C/min, quenched to −150 °C at 10 °C/min, and reheated to 200 °C at 10 °C/min.

3. Results and discussion

3.1. HMDI/DY materials as a function of hard segment content

The three HMDI/DY based TPUs which varied by only 7.2 wt% in hard segment content were found to have some similar physical properties as well as some important differences. DMA analysis (Fig. 1) provided initial insight into the structural features of this series. At temperatures below −63 °C, all three samples behaved as glassy solids with storage modulus (E') values in excess of 3×10^9 Pa. As the samples were heated, the SS phase of each went through a glass transition at ca. −50 °C. Accordingly, E' distinctly decreased as the sample passed through T_g and approached an average value of roughly 10^7 Pa. Each sample maintained approximately this level of modulus until it softened beyond the sensitivity of the DMA at temperatures in the range of 150 °C. Thus, the 'service window' for these HMDI/DY materials, as defined by the E' plateau between the soft segment T_g and the hard segment softening point, is quite broad (−30 to +150 °C) and the storage modulus is relatively temperature insensitive. The relatively high

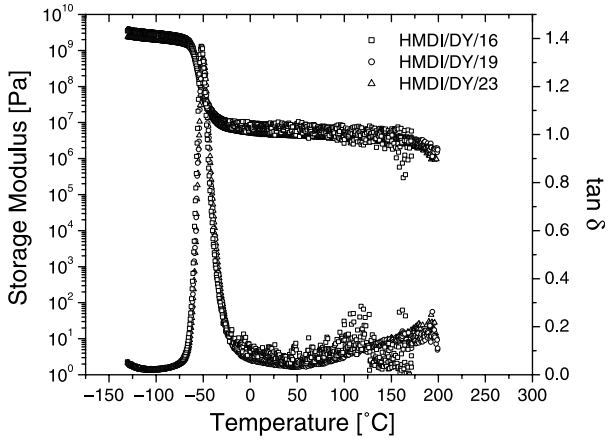

Fig. 1. Plots of E' and tan δ for the HMDI/DY/16, HMDI/DY/19, and HMDI/DY/23 systems.

modulus of the material in this region is one indication of a microphase-separated structure. The upper temperature limit of the plateau is attributed in part to the bidentate hydrogen bonding between urea linkages on adjacent HS. As noted earlier, the bond energy for bidentate bonding between urea groups has been previously calculated to be 21.8 kJ/mol [11]. As expected, HS bonding serves to enhance segmental cohesion at higher temperatures. DMA analysis (Fig. 1) clearly supports a well-defined microphase separation in these copolymers.

A microphase-separated morphology was further confirmed by SAXS (Fig. 2). Increasing the HS content in these materials promotes a corresponding increase in the volume fraction of the HS domains. This increase in volume fraction must change the microphase-separated morphology, by an increase in the size, shape or number of the microphase-separated HS domains. Here, increasing HS content results in an increase in domain spacing measured by SAXS, where materials with HS contents of 16, 19, and 23% have spacings of 84, 89 and 93 Å, respectively. This is most simply explained by an increase in domain size, as is expected in this composition range, whether from a lengthening or thickening of the hard domains. An increase in the number of domains could cause a decrease in the domain spacing, contrary to the observed shifts in the SAXS data. An attempt to attain visual evidence of the microphase-separated structure (suggested to exist by DMA and SAXS) was made with AFM. Unfortunately, none of the three samples provided clear evidence of such a structure.

While HS crystallinity was not expected in view of the asymmetric chain extender, DY, both WAXS and DSC studies gave direct support for this hypothesis. The WAXS patterns (not shown) obtained at ambient temperature of all three materials in the series showed only a diffuse amorphous halo and no sign of discrete diffraction rings attributable to a crystalline structure. Furthermore, the DSC traces of each material in the series, while showing T_gs consistent with the tan δ peak in the DMA data, showed no endothermic peaks, nor were any expected, that could be assigned to any melting of the HS phase. Representative DSC traces are shown in Fig. 3 for HMDI/DY/19.

As seen in other studies on segmented polyurethaneurea systems, increasing HS content generally leads to both higher modulus values and higher tensile strengths and can also often improve toughness in certain ranges of HS content [5,12–14]. This was also the case in these systems. A representative tensile curve for each material is presented in Fig. 4. A systematic increase occurred in each of these variables with the growing HS content. The modulus increased as expected with growing HS content as reflected by the rise in slope of the successive stress–strain curves as the HS content rose from 16 to 23 wt%. An average tensile strength for each material was determined by averaging the results of three tests. For the three HS contents 16, 19, and 23 wt%, the average tensile strengths were 10, 19 and 24 MPa, respectively. It should be noted that while higher tensile strengths with increasing HS content were expected, the increase in HS wt% from 16 to 23% led to a ca. 150% rise in tensile strength. This significant increase suggests that the level of HS phase connectivity may be quite sensitive in this HS content range. A second cause of this increase in tensile strength we believe arises from the enhanced cohesiveness of the HS domains caused by the larger average HS lengths as the HS wt% increases. The larger HS should lead to an increase in the stress the material can withstand before fracture of the material occurs.

A particularly interesting feature of these tensile curves are their nearly linear, almost Hookean stress–strain response starting at very low deformations and continuing to failure which occurs at levels of extension exceeding 600% (Fig. 4). An expanded view of three tensile samples of the 19 wt% HS material is shown in Fig. 5. At present, the

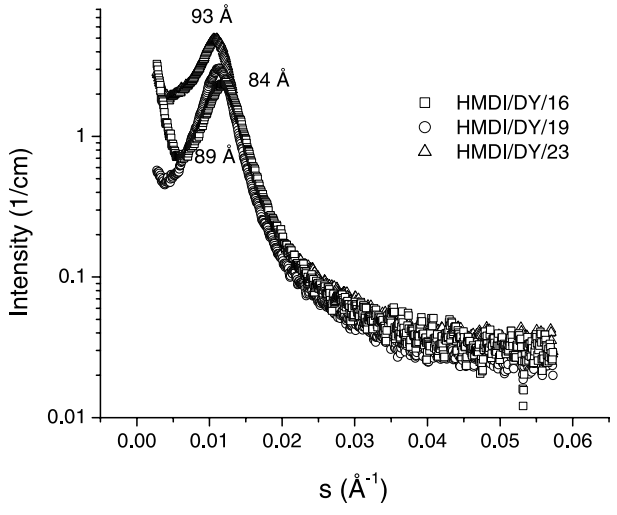

Fig. 2. SAXS scans showing first order interference peaks of HMDI/DY/16, HMDI/DY/19, and HMDI/DY/23 materials with spacings of 84, 89 and 93 Å, respectively.

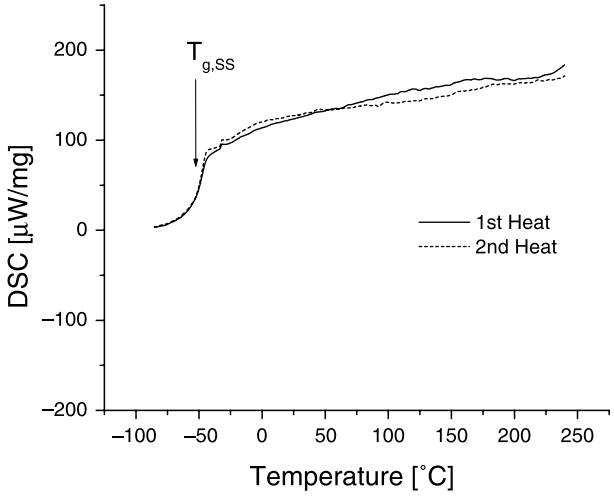

Fig. 3. DSC traces of first and second heats of HMDI/DY/19. The lack of clear melting peaks indicates that there is no detectable crystallinity.

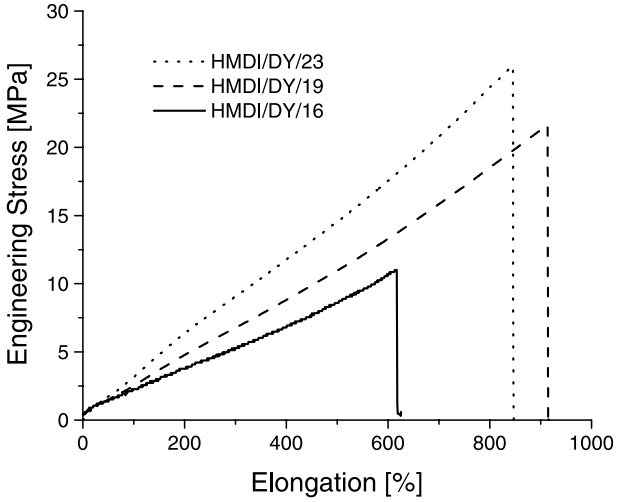

Fig. 4. Representative tensile curves of samples HMDI/DY/16, HMDI/DY/19, and HMDI/DY/23.

authors know of no other fully polymeric system that displays such near-linear behavior while undergoing tensile deformation to such high elongations. Increasing the ratio of HS to SS should also increase the toughness values, T, of these materials, which were determined by the area under the stress–strain curves. This area was calculated by integration of the stress with respect to the strain, i.e.

$$T = \int_0^{\varepsilon_B} \sigma \mathrm{d}\varepsilon \tag{1}$$

where ε_B represents the strain at break. If a Hookean behavior is assumed because these materials show nearly linear deformation, a value of the stress σ can be substituted in Eq. (1) by use of Hooke's Law,

$$\sigma = E\varepsilon \tag{2}$$

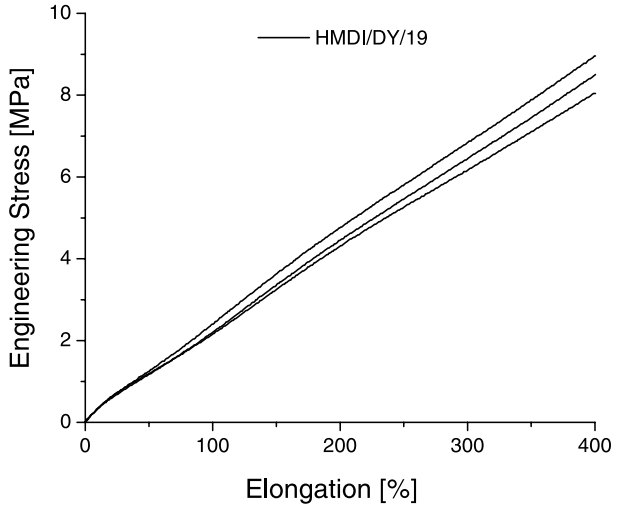

Fig. 5. Three tensile curves for sample HMDI/DY/19 show the near linear behavior beginning at low deformations.

Thus, Eq. (1) becomes:

$$T = \int_0^{\varepsilon_B} E\varepsilon \mathrm{d}\varepsilon \tag{3}$$

In Hookean behavior the modulus is constant and can be removed from the integrand leaving:

$$T = E\int_0^{\varepsilon_B} \varepsilon \mathrm{d}\varepsilon \tag{4}$$

which leads to:

$$T = \frac{E\varepsilon_B^2}{2} \tag{5}$$

Therefore, we note that, if Hookean, the toughness is directly proportional to the square of the strain in these materials. The toughness of the HMDI/DY/16, HMDI/DY/19 and HMDI/DY/23 samples was calculated to be 33, 99, and 110 MPa, respectively. As a comparison, the values calculated by integration of the area under the actual stress–strain curve were, 34, 95, and 107 MPa, respectively. Therefore, our calculated values vary only 3–4% from the integrated values thereby providing further support of the near-linear Hookean behavior these three systems display. Here again it is interesting to note that the increase in HS wt% from 16 to 23% has increased toughness values by ca. 200%.

In light of the observed near-linear stress–strain response, the hysteresis of these materials was also explored. An example of one such test on the HMDI/DY/19 material is provided in Fig. 6. Again, the Hookean type behavior was noted to begin immediately at low deformations and the response maintained near-linearity to 600% strain. The sample was then unloaded and recovered much of its initial length though the unloading response was non-linear. Note that the stress reached a value of zero before the

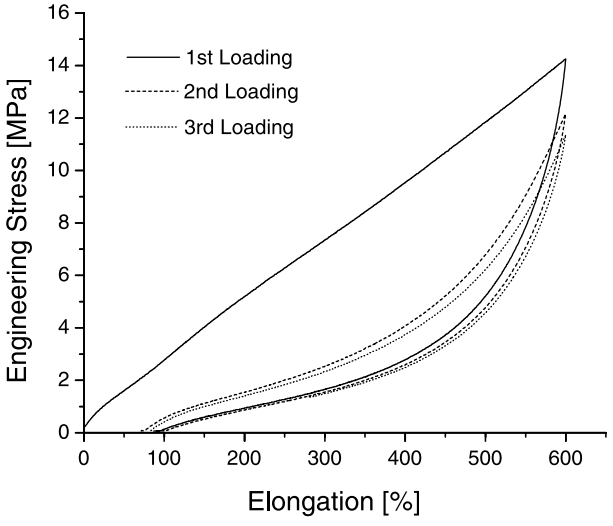

Fig. 6. Three-cycle hysteresis loops for sample HMDI/DY/19.

crosshead fully returned to its zero strain position. Therefore, there exists some amount of permanent set in the material due to the irrecoverable energy lost in the deformation. This value of set, just below 100% strain, is not, however, fully permanent. The sample continues to recover after the first loading–unloading cycle and would continue to do so if it were not immediately stretched a second time. For this reason the onset of stress during the second loading occurred at an earlier strain than where the stress dropped to zero during the first unloading cycle. Upon the second deformation, it was evident that the loading curve did not trace the previous unloading curve. Note also that the second deformation does not display the same near-linear stress–strain response of the first extension, nor was it expected to, due to the disruption of the HS structure that occurred as a result of the first loading. Clearly, considerable modification was done to the structure that was responsible for the near-linear response during the initial extension. All subsequent loading curves show strain hardening behavior and the responses are very similar to one another. This is apparent from the increase in the slope of the loading curves as the materials are again elongated to high strains. After the third and final loading–unloading cycle, the permanent set could be measured more accurately. Immediately after its removal from the testing frame, the residual strain was measured to be 2 mm, or 20%. However, 24 h later the sample had recovered almost all of its initial length at ambient temperature and was measured to be 10.5 mm in length (indicating only a 5% permanent set).

The amount of recovery found in these samples raises another question about the morphological features of these materials. Clearly, based on the hysteresis results, this morphology is softened greatly through modification of the HS phase with extension. To address how this disruption of structure influences the time dependence or relaxation behavior of the system, some stress relaxation measurements were undertaken at 600% extension—the results being shown in Fig. 7. All three materials were stretched at a rate of 100 mm/min so that the loading was completed in 36 s. After extension ended all three materials experienced stresses of ca. 20 MPa. The samples were then held at that length for at least 3 h, until the rate of change of the stress level was nearly zero. All samples show that they maintain a stress in excess of 5 MPa after this 3 h period. It appears from the curves that two very distinct relaxation mechanisms are occurring, one dominating the short time scale and a second occurring over a much longer time. While an attempt to fit the relaxation curves was made using two Maxwell models in parallel, the fit was deemed too poor to include although certainly the general character of the model captured the general shape of the observed behavior.

Having completed all of the characterization techniques discussed thus far, the ability of each material to be reprocessed was investigated, as this is an important feature of thermoplastic elastomers. Unused pieces of each material

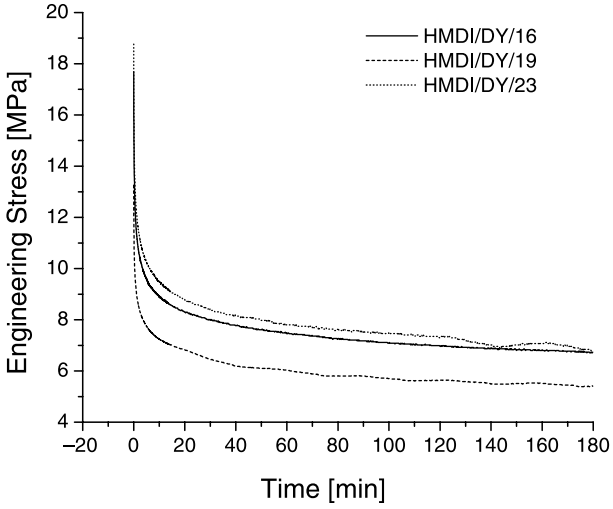

Fig. 7. Stress relaxation of the three HMDI/DY materials after an initial stretch to 600%.

were placed in a hydraulic press with platen temperatures of 200 °C. Each material was found to be easily reprocessable as the pressing resulted in a clear and uniform film for each system. The tensile properties of the remolded films were then tested for comparison with the solvent cast films (Fig. 8). The remolded films display very similar deformation properties to the solvent cast films up to 600% elongation. The modulus values are very close as the deformation curves almost lie atop one another. In addition, the unique near-Hookean linearity of the curves at low levels of deformation is maintained after remolding. Also important is the fact that the remolded materials retain the characteristic of high recoverability.

The similarity in mechanical behavior is an important observation given the different physical and thermal histories of the samples. In some block copolymer systems, such as many of the SBS triblock materials, solvent cast

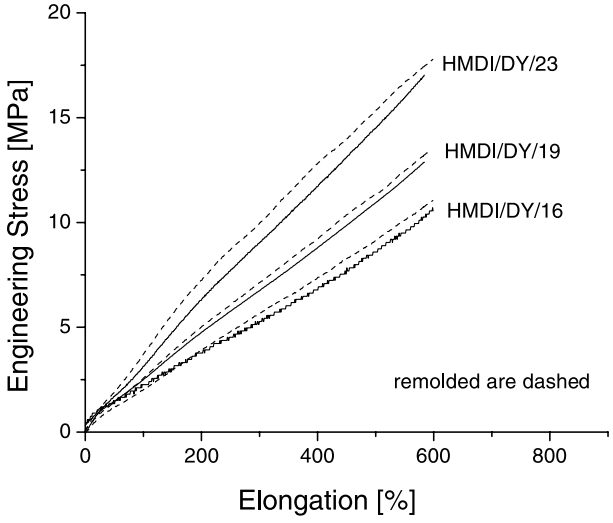

Fig. 8. Tensile curves of HMDI/DY materials comparing solvent cast and remolded materials.

materials have been shown to contain very different structure than their melt processed counterpart [15,16]. In this case, the HMDI/DY films appear to have a comparable structure, irrespective of whether they were produced with the THF/IPA solvent or have a melt history.

3.2. HDI/EDA/8 and HDI/DY/9 materials

The two final materials, HDI/EDA/8 and HDI/DY/9, differ from those previously discussed in two respects. First, the latter two were prepared using HDI as the diisocyanate in place of HMDI and second, EDA (symmetric) was chosen as the chain extender for one of the samples as opposed to DY (asymmetric) thereby allowing the effect of chain extender symmetry to be examined. In order to understand the influence of chain extender structure and symmetry on the properties, both samples were prepared with the same molar compositions, which is [HDI]/[Kraton]/[CE] = 3/2/1. The difference in the HS content comes from the higher MW of DY.

The DMA traces of these two samples (Fig. 9) show results somewhat similar to the HMDI/DY systems with regard to the SS T_gs. In this case, the respective SS T_gs are −53 °C for HDI/DY/9 and −54 °C for HDI/EDA/8. As the sample is heated through T_g the material softens considerably and E' decreases from ca. 10^9 Pa to ca. 10^7 Pa, the same general range of values as noted for the HMDI/DY materials. As with the HMDI/DY samples, the magnitude of the modulus in the plateau region is ascribed to the presence of a microphase-separated structure. An additional conclusion can be drawn based on the similarity of the modulus values of these two sets of materials. Recall that the HDI based materials have a much lower HS content (ca. 8% as opposed to 16–23%). This implies that the HDI/DY/9 and HDI/EDA/8 materials must have some level of higher interconnectedness of the hard microphase to account for the similar E' values. This issue will be further addressed later in this report.

These materials also display distinct differences from the HMDI/DY materials. Following the SS T_g, there is a relatively flat and broad plateau in modulus between −30 and +100 °C, a smaller thermal window than was observed for the HMDI/DY systems. Therefore, the plateau in these materials spans only 130 °C compared to the 180 °C span of the HMDI/DY materials which possessed both longer HS and a higher HS content. Recall from Table 1 that the HMDI based materials had HS M_n values between 645 and 1020 g/mol whereas the HDI/DY/9 and HDI/EDA/8 have HS M_n values of 320 and 280 g/mol, respectively. The breadth of the rubbery plateau is again due in part to the bidentate hydrogen bonding between urea linkages on adjacent chains. Though each set of polyurethaneureas contains both monodentate and bidentate hydrogen bonds, the combined effect of the lower HS contents and lower HS molecular weights in the HDI based materials is to reduce the number of urea linkages available for bonding. The smaller number of hydrogen bonds is expected to lower the upper temperature limit as the HS domains of the HDI materials begin to soften sooner than their HMDI based counterparts. The use of HDI rather than HMDI may also influence differences in hard segment cohesiveness/packing behavior. Specifically, this reduction in upper temperature modulus could also be due to the melting of the symmetric HDI, although no direct evidence of a crystalline HS was obtained for either material as will be addressed shortly. Above 100 °C the materials each began softening until ca. 150 °C, where both have softened beyond the sensitivity of the DMA. Two key differences are also apparent in the temperature dependent tan δ responses of the HDI/DY/9 and HDI/EDA/8 materials. The first difference is the very small peak at ca. 25 °C in the HDI/EDA/8 sample. This peak disappears after annealing at 100 °C and may result from residual solvent in the freshly cast material even though this sample had been given the same preparation history as the others. The second difference, unaffected by annealing, is the disparity in magnitude of the tan δ peak at the T_g for these materials. The peak in HDI/DY/9 sample has a magnitude of ca. 1.2 while the HDI/EDA/8 sample has a peak value of ca. 0.9. While not excessively large, this roughly 20% difference in peak height coupled with the similar peak breadths, does imply that the soft segment phase of the HDI/DY/9 sample is less restricted in its motion than the soft segment phase of its HDI/EDA/8 counterpart. It might also be noted that the breadth of the tan δ peaks are essentially the same.

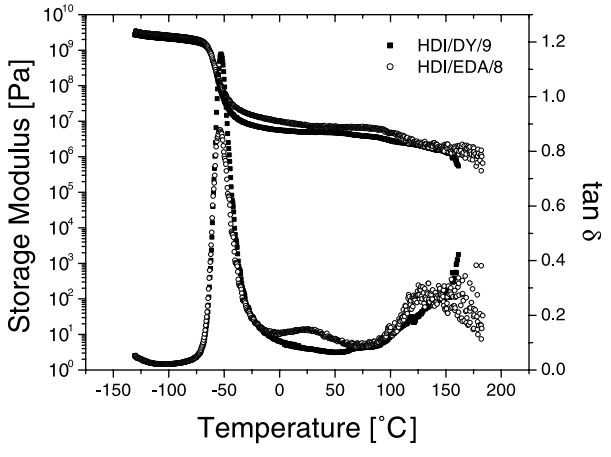

Fig. 9. Plots of E' and tan δ for the HDI/EDA/8 and HDI/DY/9 samples.

The microphase-separated morphologies of both the HDI/EDA/8 and HDI/DY/9 materials were further confirmed by SAXS measurements (Fig. 10). From those scans, well-defined first order interference peaks were observed at 123 and 125 Å, respectively. However, the angular locations of these peaks raise a distinct question. Why are the spacings of these lower HS content materials appreciably larger than the HMDI series discussed previously, which had spacings of 84–93 Å? One tentative explanation is that the difference may be due to, what is on average, a shorter

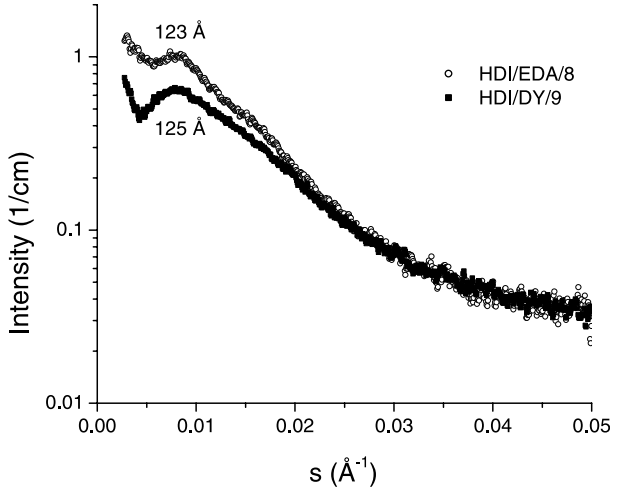

Fig. 10. SAXS scans showing first order interference peaks for the HDI/ED/8 and HDI/DY/9 materials with spacings of 123 and 125 Å, respectively.

overall HS length in the HDI series. This may result in some of the shortest hard segments dissolving into the SS phase. Indeed, based on the M_n of these segments, they are only 1–3 segments long indicating that dissolution of hard segments may be more likely in these materials. Dissolved HS could effectively lengthen the SS (doubling the effective SS molecular weight to ca. 6600 g/mol), resulting in a larger spacing. In addition to shifting the location of the peaks to smaller angles, some dissolved HS would broaden the interference peaks in the SAXS profiles. This observation for the HDI materials (recall Fig. 10) lends further support to the explanation proffered.

While it is clear from both the DMA and SAXS data that microphase-separation occurs for each material, the exact morphology of the hard phase is not obvious. In further examination of the HDI based materials, neither WAXS nor DSC (Fig. 11) showed any evidence of crystallinity for either sample. This is qualified with the understanding that the very low levels of HS content may make any crystalline structure that might exist exceedingly difficult to measure.

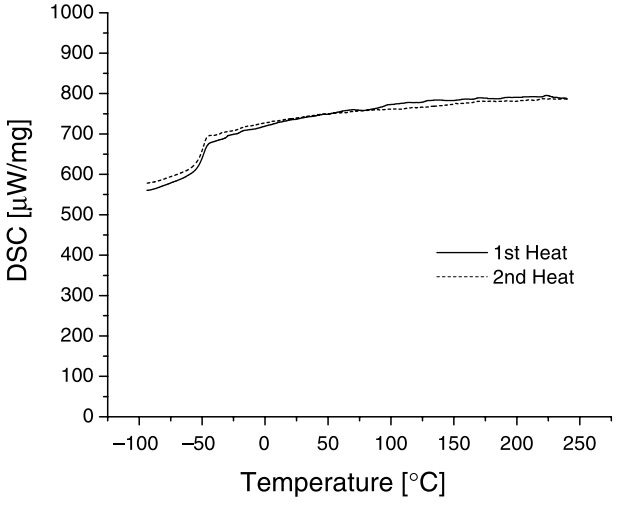

Fig. 11. DSC trace of HDI/DY/9 sample showing no evidence of crystallinity.

In the interest of obtaining visual evidence of the microphase structure, AFM was employed. AFM phase images were obtained of a well-percolated HS microphase-separated structure for both samples. Fig. 12(a) shows the very clear thread-like structure of HDI/DY/9 while Fig. 12(b) shows the stranded structure of HDI/EDA/8. The three images provide direct visual evidence of two distinct phases: A well-dispersed, interconnected, stranded or thread-like hard phase represented by the light portions of the image, embedded in a soft segment matrix represented by the darker portions of the image. As noted earlier, the DMA behavior of the HDI/EDA/8, HDI/DY/9 and the three HMDI/DY materials gives reason to believe that they have somewhat similar microphase-separated structures, despite obtaining clear AFM scans only for the two HDI based samples. In addition to the cast film samples discussed thus far, a second film sample of HDI/EDA/8 was obtained by remolding unused portions of the solution cast material in a hot film press. After molding, AFM was performed on the films and the same percolated, microphase-separated structure was found to exist in these films indicating that the material can be reprocessed although the level of HS percolation appears to be somewhat less than within the solvent cast film (Fig. 13).

Despite the similarities between the HDI/EDA/8 and HDI/DY/9 samples discussed thus far, there is a surprisingly large difference in the materials with respect to their ambient stress–strain properties. Representative stress–strain curves are shown for each material in Fig. 14. Both materials display a deviation from linearity at low strains followed by essentially linear behavior until break. The tensile curves also show the HDI/DY/9 material to have over twice the tensile strength of the HDI/EDA/8 material, i.e. 13 versus 5.5 MPa. Furthermore, the HDI/DY/9 sample achieves higher strains at break, 2000 versus 1200%, than the HDI/EDA/8. Lastly, the HDI/DY/9 material displayed a toughness more than three times greater than that of the HDI/EDA/8 sample, 141–43 MPa, respectively.

The tensile properties of the remolded materials were also measured. Again, the remolded DY based material behaves similarly to the solvent cast material, the tensile curves having roughly the same shape. However, the remolded material does not achieve the same ultimate stress. Consistent with the AFM images, the lower stresses achieved in these tests support the speculation that there is less percolation of the hard segment phase throughout the remolded samples.

4. Conclusions

Novel segmented polyurethaneurea copolymers based on HMDI, an ethylene–butylene soft segment and HS contents

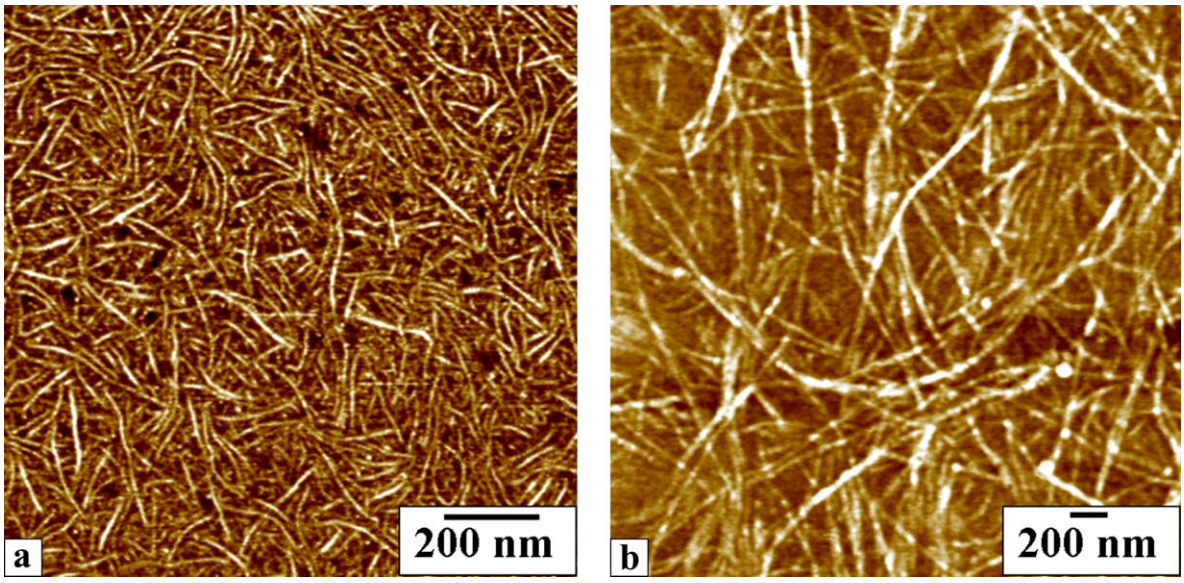

Fig. 12. (a) AFM phase image of HDI/DY/9 sample showing a well percolated nano-stranded morphology. (b) AFM phase image of HDI/EDA/8 showing nano-stranded morphology.

between 16 and 23% were prepared. These materials, developed microphase separated morphologies with wide service windows as measured with SAXS and DMA. In addition to the broad temperature insensitive E' plateau, they each displayed a unique, near linear, Hookean-like stress–strain response until fracture at very high levels of strain, in excess of 900% in some cases. The materials were found to be reprocessable as new clear, transparent films were made by melt pressing unused portions of the solvent cast material. The remolded materials were found to display the same near-linear, Hookean behavior upon deformation. The similarities in tensile behavior indicate that similar microstructures are attained for these materials whether they are fabricated as a result of solvent casting or melt pressing.

Ethylene/butylene based segmented polyureas were also synthesized using HDI as the diisocyanate and EDA or DY as the chain extender. These materials had HS contents between 8 and 9%. Both also developed percolated, thread-like microphase-separated morphologies with broad service windows, though less broad than the HMDI materials. The more narrow service window is attributable to the lower HS content and shorter HS length in the HDI based materials. This necessarily reduces the number of bidentate bonds in the material and lowers its upper temperature limit. The shorter HS is also thought to be responsible for the different

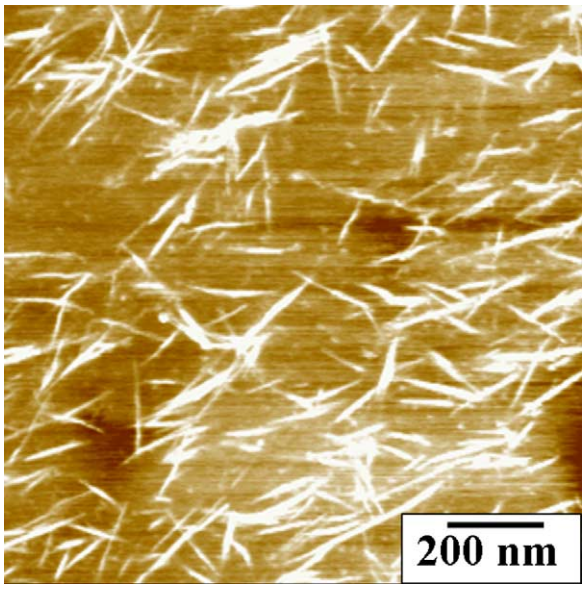

Fig. 13. AFM phase image of HDI/EDA/8 after remolding in a hot press at 200 °C.

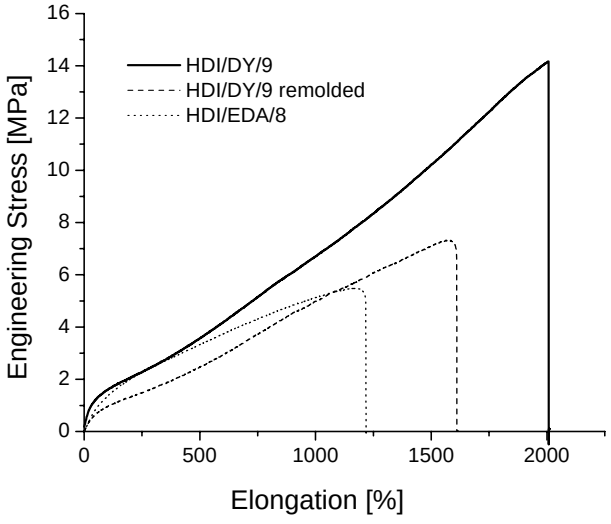

Fig. 14. Tensile curves of HDI materials comparing solvent cast and remolded materials.

interdomain spacings as measured with SAXS, whereby the shorter HS leads to dissolution of some hard segments into the SS matrix and 'effectively lengthens' the SS, shifting the interference peak to higher length scales. Direct visual evidence of the microphase-separated morphology was obtained by AFM for each of the HDI based materials. Each of these materials was also found to be reprocessable in a melt press as well, producing clear, uniform films.

References

[1] Bruins PF. Polyurethane technology. New York: Interscience Publishers; 1972.
[2] Doyle EN. The development and use of polyurethane products. New York: McGraw-Hill; 1971.
[3] Abouzahr S, Wilkes GL. Segmented copolymers with emphasis on segmented polyurethanes. In: Folkes MJ, editor. Processing, structure and properties of block copolymers. London: Elsevier Applied Science Publishers; 1985.
[4] Tyagi D, Wilkes GL. Morphology and properties of segmented polyurethane–urea copolymers prepared via *t*-alcohol 'Chain Extension'. In: Lal J, Mark JE, editors. Advances in elastomers and rubbery elasticity. New York: Plenum Press; 1986. p. 103–28.
[5] Gisselfaelt K, Helgee B. Macromol Mater Eng 2003;288(3):265–71.
[6] Singh A. Adv Urethane Sci Technol 1996;13:112–39.
[7] Oertel G. Polyurethane handbook: Chemistry, raw materials, processing, application, properties. New York: Hanser Publishers; 1985.
[8] Sheth JP, Yilgör I, Yilgör E, Wilkes GL. Polym Prepr (Am Chem Soc, Div Polym Chem) 2004;45(1):562–3.
[9] Kazmierczak ME, Fornes RE, Buchanan DR, Gilbert RD. J Polym Sci, Part B: Polym Phys 1989;27(11):2173–87.
[10] Bates FS, Fredickson GH. Phys Today 1999;32–8.
[11] Yilgör E, Burgaz E, Yurtsever E, Yilgör I. Polymer 2000;41:849–57.
[12] Amitay-Sadovsky E, Komvopoulos K, Ward R, Somorjai GA. Appl Phys Lett 2003;83(15).
[13] Harris RF, Joseph MD, Davidson C, Deporter CD, Dais VA. J Appl Polym Sci 1990;41(3–4):509–25.
[14] Lin SB, Hwang KS, Tsay SY, Cooper SL. Colloid Polym Sci 1985; 263(2):128–40.
[15] Bagrodia S, Wilkes GL. J Biomed Mater Res 1976;10:101–11.
[16] Huang H, Hu Z, Chen Y, Zhang F, Gong Y, He T, et al. Macromolecules 2004;37(17):6523–30.